New Journal of Physics
The open access journal at the forefront of physics

Deutsche Physikalische Gesellschaft DPG IOP Institute of Physics

PAPER • OPEN ACCESS

An accurate and robust metrological network for coherent optical frequency dissemination

To cite this article: Etienne Cantin *et al* 2021 *New J. Phys.* **23** 053027

New Journal of Physics
The open access journal at the forefront of physics

Deutsche Physikalische Gesellschaft DPG
IOP Institute of Physics

Published in partnership with: Deutsche Physikalische Gesellschaft and the Institute of Physics

CrossMark

OPEN ACCESS

RECEIVED
8 November 2020

REVISED
5 February 2021

ACCEPTED FOR PUBLICATION
18 February 2021

PUBLISHED
18 May 2021

PAPER

An accurate and robust metrological network for coherent optical frequency dissemination

Etienne Cantin[1,2,*], **Mads Tønnes**[1], **Rodolphe Le Targat**[1], **Anne Amy-Klein**[2], **Olivier Lopez**[2] **and Paul-Eric Pottie**[1]

[1] LNE-SYRTE, Observatoire de Paris, Université PSL, CNRS, Sorbonne Université, 61 av. de l'Observatoire, 75014 Paris, France
[2] Laboratoire de Physique des Lasers, Université Sorbonne Paris Nord, CNRS, 99 av. J.B. Clément, 93430 Villetaneuse, France
[*] Author to whom any correspondence should be addressed.

E-mail: etienne.cantin@univ-paris13.fr

Keywords: frequency transfer, metrology, fiber optic links, laser optics, interferometer

Supplementary material for this article is available online

Abstract

We introduce multi-branch repeater laser stations (MLSs) for the dissemination of an ultra-stable signal from one point to multiple users and the simultaneous evaluation of the stability and accuracy of multiple links. We perform the study of the noise floor of this new instrument. We present then an optical fiber network of 4800 km built with three MLSs and 13 repeater laser stations (RLSs). We show the multi-user optical frequency dissemination on four links totalizing 2198 km with uncertainties below 1.1×10^{-19}. The robustness of the network over two years is presented and stability and accuracy at 10^7 seconds integration time are finally showed.

1. Introduction

Optical fiber links enable the accurate and ultra-stable transfer of an optical frequency reference on distances of more than 1000 km [1–5]. They include an active or passive correction of the noise added through the fiber propagation leading to uncertainties in the range of 10^{-20} or even below [3, 6]. It is thus an unavoidable technique for the accurate comparison of distant optical clocks [7, 8] and their applications to chronometric geodesy [9] and search for new physics [10]. Moreover it provides an input reference frequency signal for a wide range of precision measurements from spectroscopy [11–15] to geophysics [16–18] and syntonisation in astrophysics [5, 19].

Since a few years, the number and length of optical links increased in order to connect national metrological institutes (NMIs) or laboratory users and extend the possible applications. These links are mainly point-to-point links connecting two NMIs or an NMI and a user. However, comparison of multiple clocks in multiple NMIs requires the development of an NMI network, with the possibility of coherent dissemination between all the NMIs. It will enable not only to make significant advances in fundamental metrology but also to search for dark matter [20] or test new physics. Moreover, the development of fiber networks will provide ultra-stable frequency dissemination to many labs and institutes, and thus broaden the range and number of precision experiments.

For that purpose in-line extraction has first been proposed [21] and demonstrated in 2014 [21–23]. It is mainly suitable for dissemination to users along a main link, e.g. using a ring topology in an urban area. Nevertheless, building a fiber link network also requires some hub in order to transfer the signal from an NMI to multiple users and to develop a star, a tree or a mesh network topology.

Here we demonstrate a fiber network operated with multi-branch laser stations (MLSs) which enable coherent dissemination of an ultra-stable signal from one point to multiple users and simultaneously assess the stability and accuracy of the multiple links. It is part of a national metrological network called REFIMEVE+ [24] which aims to disseminate an ultra-stable and accurate signal generated at LNE-SYRTE to around twenty labs across France and to connection points to European NMIs. Fields of study of REFIMEVE+ concern high-resolution spectroscopy, measurements of fundamental constants, remote laser

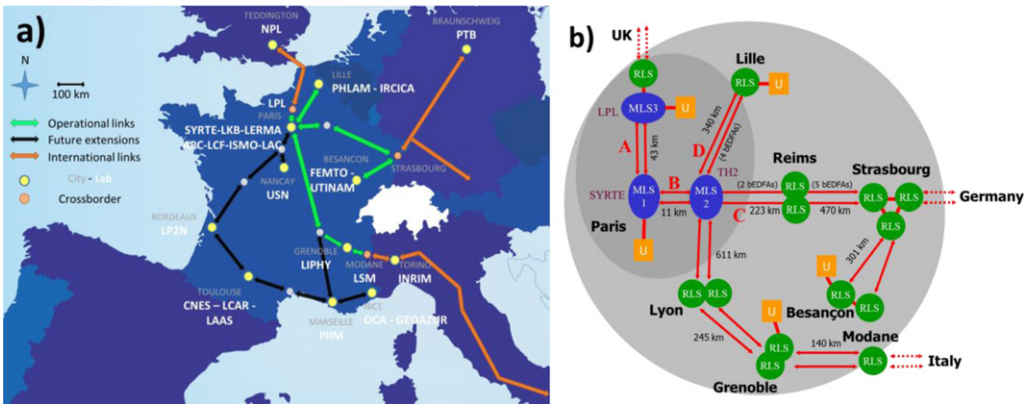

Figure 1. (a) REFIMEVE+ metrological network in France with laboratories currently benefiting from the signal. (b) Sketch of the network architecture, MLS: multi-branch laser station, RLS: repeater laser station, bEDFA: bidirectional erbium doped fiber amplifier, U: user.

stabilization or stability assessment and more generally high-precision atomic and molecular spectroscopic measurements. Together with the repeater lasers stations (RLSs) [25] already demonstrated and used for ten years, the MLS allows us to build a robust metrological network of twice 2400 km with state-of-the-art accuracy and stability.

In this paper, we first present the metrological network we are implementing on the fiber network of RENATER, the French National Research and Education Network (NREN) and the various equipment required for the signal dissemination. Then we describe the principle of the MLS, its design and the functions it provides, from the noise compensation to the assessment of the residual instability of a link. Next, we give the resulting performance of optical links driven by such MLSs, in terms of stability, accuracy and robustness and uptime. In conclusion, we give some perspectives of new applications opened by this work.

2. Implementation of an ultra-stable optical link network on the RENATER fiber network

Figure 1(a) displays the current status of the REFIMEVE+ metrological network and its European connections. Besides regional dissemination inside the Paris area and especially to LPL [6], it includes four optical links to Lille [25], Strasbourg [2], Besançon and Modane. It totalizes 4802 km of coherent optical frequency links. The link lengths range from 11 to 1000 km with attenuation up to 262 dB. Connections with European links to PTB in Germany, NPL in the UK and INRIM in Italy happen respectively at Strasbourg [4, 7], LPL [10] and Modane. Operation of the whole network will be reported elsewhere. We will restrict this paper to the study of the MLSs and the links to LPL, Lille and Strasbourg.

Figure 1(b) shows the network design with three nodes including an MLS at LNE-SYRTE, LPL and TH2 (a data center in Paris). The network is fed with an ultra-stable laser, with a linewidth about 200 mHz. The drift of the ultra-stable laser is measured against an active H-Maser using an optical frequency comb. This drift is actively suppressed applying a correction via a programmable radio peripheral platform (ETTUS), which slope is updated every 30 s, resulting in a residual drift smaller than 10 mHz s^{-1} at all times [26]. The whole network is based on cascaded links using remote control of servo loops, gain parameters and measuring devices. This gives the possibility to compensate for the large noise and attenuation, and, moreover, to improve the short-term noise rejection, which is limited by the round-trip propagation time in each segment [25, 27].

Active noise compensation (ANC) is implemented on each link using the Doppler noise compensation technique [27]. Both the bandwidth and the amplitude of the correction are limited by the roundtrip propagation delay [27], giving rise to typical residual instabilities around 10^{-15}–10^{-17} at 1 s averaging time. This residual noise is evaluated using a second parallel link, denoted as down-link, in order to send back the signal transferred with the first optical link, denoted as up-link, to the input lab as depicted in figure 2 (see supplementary material for detailed explanation (https://stacks.iop.org/NJP/23/053027/mmedia)). One can thus detect the so-called end-to-end beat-note between the input signal and the signal transferred by the up-link and down-link successively. The frequency of this beat-note is counted and it gives an upper value of the stability and accuracy of each link [4].

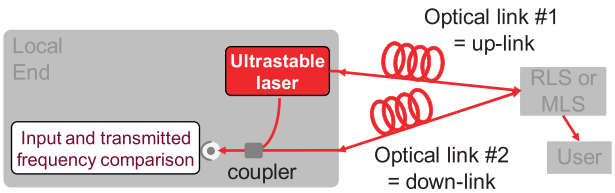

Figure 2. Principle of an optical link with simultaneous assessment of the residual noise and accuracy. The input and transmitted frequency comparison, so-called end-to-end measurement, gives an upper value of the up-link and down-link stabilities and accuracies (see supplementary for details).

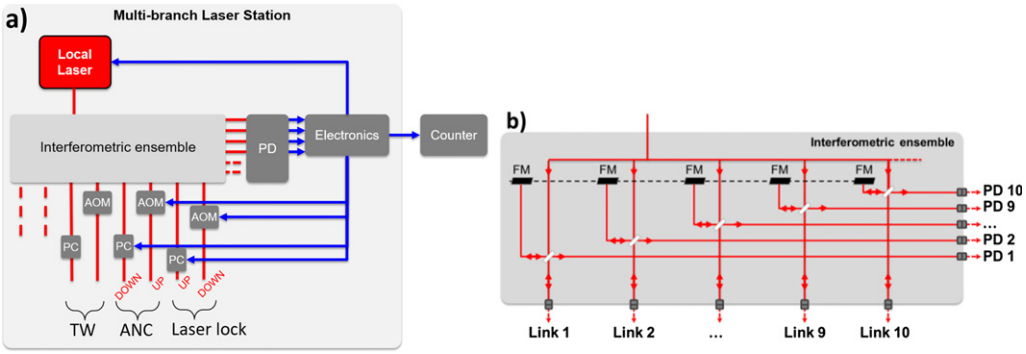

Figure 3. (a) Schematic of a multi-branch laser station (PD = photodiode, PC = polarization controller, AOM = acousto-optic modulator, TW = two-way, ANC = active noise compensation). (b) Schematic of the interferometric ensemble (FM = Faraday mirror, PD = photodiode).

The optical links are implemented on the fiber network of RENATER. The metrological signal is transferred on a dedicated frequency channel of bandwidth 100 GHz centered at wavelength 1542.14 nm (channel #44 of the International Telecommunication Union Grid). It is multiplexed with the data traffic using optical add-drop multiplexer. The propagation of the metrological signal is fully bidirectional using dedicated bidirectional optical erbium-doped fiber amplifiers (bi-EDFAs), and RLSs [2, 4, 25]. At the network output ends, a user module can be connected to an RLS and enables any user to get an ultra-stable signal with noise correction up to this module. MLS, RLS and bi-EDFAs are remotely controlled. Their supervision is integrated into the network operating center of RENATER. Bidirectional amplifiers, RLSs and user modules are now commercially available [25].

3. The multi-branch laser station

3.1. Principle and description

In order to transfer the signal to several points, the network includes three MLSs. These stations are based on the RLS principle [2, 25] and includes new functionalities which are mainly multiple link coherent dissemination and residual noise measurement (figure 3(a)). It provides several coherent outputs which are all copying the ultra-stable input signal. In addition, this device can compensate for up-link noise, controls polarization and verifies in real time the performance of each down-link independently.

An MLS includes a laser, a multi-branch optical interferometric ensemble, electronic boards to lock the laser and the up-links and a control rack to control the down-links and to assess the locking performance. The local laser is divided in the interferometric ensemble (gray part) into 8 to 12 coherent ports which feed several fiber links (bottom of the figure). The multi-branch low-noise interferometric ensemble (figure 3(b)) is designed to detect the beat-notes of the same optical phase of the laser with several external optical signals. It includes several reference arms of similar optical length, each combined with an external optical port that corresponds to the second arm of a highly unbalanced Michelson interferometer, thus providing several phase-coherent two-arm interferometers. Such an interferometric ensemble is also suitable for multi-branch optical frequency comb.

The dissemination configuration is fully versatile. It can be achieved either by ANC of the fiber noise, or by a two-way technique, or by a combination of the above techniques (as illustrated in [6]).

The local laser is phase-locked on the incoming metrological signal using one of the two-arm interferometers. The other interferometers are used in pairs to establish up and down-links to transfer the

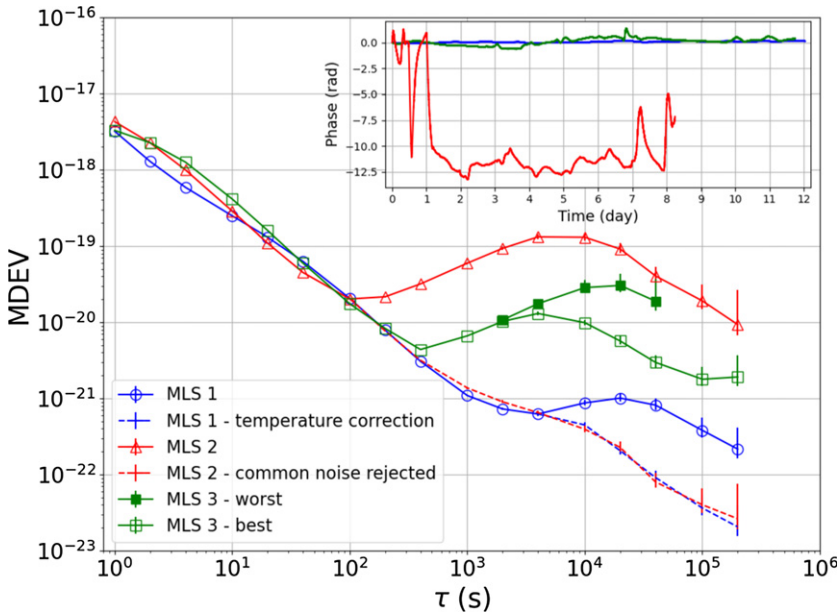

Figure 4. Characterization of the noise floor of the multi-branch interferometric ensemble of the different MLSs. Fractional stability versus averaging time of the free space interferometer from MLS1 (blue circles) and from ML2 (red triangles) without (continuous line) and with (dashed line) correction or common noise rejection and of the free space interferometer from MLS3 (green squares). Inset: phase fluctuations of the three measurements (one optical cycle lasts 5 fs).

signal to a remote location (up-link) and check the quality of the transfer using the second link (down-link). The beat-note between the local laser and the signal received after the round-trip propagation through the up and down-link gives a measurement of the out-of-loop end-to-end residual noise. It is filtered and sent to an external counter (electronics part on the right of figure 3(a)). For the up-link, it includes an AOM for noise correction. For the down-link, it includes a polarization controller, which is required for the automatic maximization of the beat-note amplitude. The beat-notes are detected, filtered and used for either a servo-loop, noise measurement or frequency counting. It uses the multifunction electronic board developed for commercial RLSs [25] for the laser and link stabilization. For the detection and polarization optimization of the measurement system, it uses specifically designed homemade electronic boards.

The MLS can be designed in order for the noise compensation to be insensitive to the frequency fluctuations of the local RF oscillator [2, 25, 28]. In that case, an acousto-optic modulator with a proper frequency shift is inserted in the multi-arm interferometer. Such MLS can be used outside a lab, for instance in a telecommunication node, without the need for accurate atomic clocks or a GNSS signal.

We benefit from the development performed for the RLS to supervise the operation of the MLS [2, 25]. Notably every lock, or relock, is automatic and can be controlled remotely. Detailed description of the electronic processing and control can be found in [25]. Moreover, the robustness and reliability of the link stabilization system of the MLS is insured by industrial-grade components, tested and validated in the field, and by the availability of spares for fast replacement. The result is a plug and play equipment, which was operational the day after it was installed in the network and shows very high uptime (see section 4).

As shown in figure 1, we built and set up three MLSs (see supplementary material for technical details). The first two MLSs, denoted MLS1 and MLS2 on figure 1, include a free space interferometric ensemble for optimal noise floor. They are set up at the input end of the REFIMEVE network at LNE-SYRTE and at TH2 respectively, and are used as nodes of a star national network. MLS2 includes an acousto-optic modulator in order to reject the noise of the local RF oscillator.

The last MLS is set up at LPL (MLS3 in figure 1) and is used for local dissemination inside the lab [13, 15] and for frequency comparison with the signal arriving with another fiber link from NPL [29]. It includes a fibered interferometer ensemble.

3.2. Performance

Figure 4 shows the noise floors of the multi-branch interferometric ensembles of the MLSs, which give the best possible performance of any ultra-stable frequency transfer or comparison.

This noise floor was measured by connecting two optical ports of the same multi-branch interferometric ensemble, thus being an out-of-loop measurement. This way we connect two interferometers with a short

fiber, sharing then the same external arm and we realize a two-way frequency comparison using the same laser source [30, 31]. The beat-note signal of both interferometers were counted with a dead-time free frequency counter in lambda-mode [32, 33] and post-processed to obtain their half difference. It is free from laser noise and from the noise of the shared fiber and exhibits the residual noise of the interferometers, known as interferometric noise [34, 35]. This noise is expected to arise from the mismatch of the optical lengths between the laser output and each interferometer, including the paths to the interferometer couplers and the short reference arms.

The free space interferometers of MLS1 exhibits the lower noise floor, as shown with blue circles in figure 4. The stability is 3.2×10^{-18} at 1 s averaging time, it decreases to 6.2×10^{-22} at 4000 s before increasing to 1×10^{-21} at 20 000 s averaging time. The corresponding phase fluctuations are shown in the inset in blue. To the best of our knowledge, this is a record noise floor for optical link noise detection. The thermo-optic sensitivity is almost completely suppressed. Moreover, the long-term stability can be reduced to 2.5×10^{-23} by post-processing the data taking into account the temperature variations [6]. In addition, we have tested this MLS1 on a dedicated test-bench and we have demonstrated that all the outputs of the interferometric ensemble show the same performance in a simulated link and can then be used independently.

The noise floor of the interferometric ensemble of MLS2, which is free space and includes an AOM, is displayed as red triangles in figure 4. This measurement has been realized in the field at TH2 data center. The stability starts at 4.3×10^{-18} at 1 s averaging time and reaches a noise floor of 2×10^{-20} at 100 s averaging time before increasing to 1.2×10^{-19} at 10 000 s averaging time. We have determined that it is limited by the phase fluctuations occurring in the AOM [36]. The corresponding phase fluctuations are shown in the inset in red. By correlating those phase fluctuations with an additional simultaneous measurement between a pair of other outputs, we can reject the common fluctuation sources of the two measurements, including the ones from the AOM, as shown with the dashed red line. This result by post-processing is consistent with the blue dashed line as expected.

The green squares in figure 4 show the modified Allan deviation (MDEV) for the fibered interferometric ensemble of MLS3 in two different cases. Open squares correspond to a measurement using two ports of the last coupler of the interferometric ensemble, thus showing the maximum noise correlation between outputs and giving the best stability limit of the noise floor of this MLS. The corresponding phase fluctuations are shown in the inset in green. Full squares correspond to a measurement between two different branches after the first coupler of the interferometric ensemble, thus showing the minimum correlation between outputs, thus giving the worst stability limit of the noise floor. The stability starts at 3.3×10^{-18} at 1 s averaging time and reaches a minimum of 4.4×10^{-21} at 400 s averaging time. Then it increases due to the temperature fluctuations of the interferometric ensemble. For the worst case, it shows a maximum of 3×10^{-20} at 20 000 s averaging time, whereas the bump is reduced to 1.3×10^{-20} at 4000 s averaging time for the better case, and the long-term stability reaches 2×10^{-21} at 200 000 s averaging time. Note that the noise arising from local temperature variation can be partially compensated in post-processing [6].

We can notice that the MLS3's interferometric noise limitation occurs one order of magnitude higher than that of the MLS1 interferometer, emphasizing the fact that fibered interferometers are more sensitive to thermal fluctuations than free space ones.

For all three MLSs, the interferometric noise is low enough for long-haul frequency dissemination and comparison, as shown in section 4. The ultra-low noise interferometric ensemble of MLS1 is especially suitable for relatively short fiber links where the noise rejection is very high. Alternatively, fibered interferometers are easier to realize and can be used for long-haul fiber links or frequency transfer at the 10^{-19} level. The noise floor of MLS2's interferometric ensemble is dominated by the phase fluctuations induced by the AOM. Its design could be improved in the future.

4. Results

We present the experimental end-to-end data acquired with the REFIMEVE+ network at LNE-SYRTE and at the central node of the network, located at the TH2 data center. The ultra-stable optical reference signal is transferred with four optical links to the remote ends, located at the TH2 data center, LPL, Lille and Strasbourg. The RLS or MLS transfers the signal back to the input end with a second fiber link. We record the end-to-end frequency fluctuations of the beat note between the returned signal and the original signal of the MLS. Table 1 displays the main characteristics of each fiber link, ranging from 22 to 1410 km, and denoted as A to D on figure 1(b). The A, B and D links are two segment fiber links (for instance SYRTE–LPL and LPL–SYRTE for link A) whereas the C link is a cascaded link of four segments (Paris–Reims, Reims–Strasbourg, Strasbourg–Reims and Reims–Paris). Link C uses home-made RLSs [2] whereas link D uses commercial RLSs [25].These links are operated simultaneously.

Table 1. Length, number of segments, number of amplifiers and losses for the four links using MLSs and sketched on figure 1(b).

	Distance (km)	Number of segments	Number of EDFAs	Total fiber losses (dB)
A: SYRTE–LPL–SYRTE	2 × 43	2	0	45
B: SYRTE–Paris–SYRTE	2 × 11	2	0	16
C: Paris–Strasbourg–Paris	2 × 705	4	2 × 7	410
D: Paris–Lille–Paris	2 × 340	2	2 × 4	160

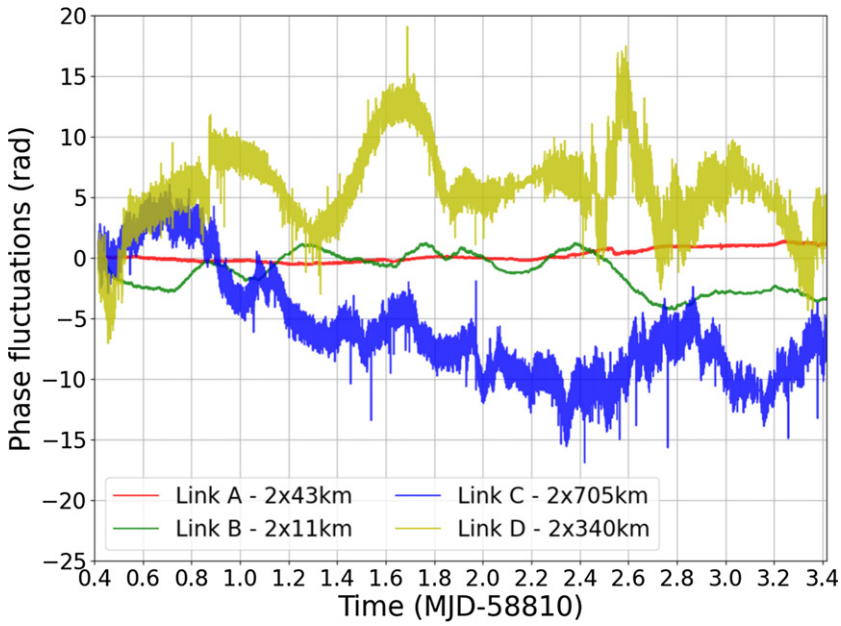

Figure 5. End-to end phase fluctuations of the four links using MLSs during 3 days. Data are recorded with 1 s gate time.

4.1. Experimental data at a few days

We discuss first the situation of data recorded during a period of almost continuous operation of the four links. We process the end-to-end data with similar procedure described in [37]. The residual phase fluctuation is calculated from the integration of the frequency fluctuations over the time. Figure 5 displays the phase variations of a 3 days measurement duration without significant missing data. The uptimes for the links A to D are respectively 97.3%, 97.9%, 98.1% and 93.0%. Note that better uptime and lower uncertainty can be achieved after dedicated optimization of the links and extensive data analysis [25].

We observe much lower noise for the shortest links (red, 86 km and green, 22 km), as expected. For this period, the phase wanderings over 3 days for the links A to D are respectively 1.1 rad, 3.4 rad, 7.0 rad and 3.2 rad (one optical cycle lasts 5 fs).

Figure 6 shows the corresponding relative frequency stability, with the same color code. All the links integrate with a slope of $\tau^{-3/2}$ until about 20–100 s integration time, showing the coherent regime. The 1 s MDEV are 2.0×10^{-17}, 1.7×10^{-17}, 5.9×10^{-16} and 5.4×10^{-16} for the links A to D respectively. The free running noise of the first span of each of the links are reported on figure 6, as dashed lines, with the same color code. We observe that it differs from one link to the other and does not simply scale with the length. In particular, one notices that for the two short links (A and B, red squares and green bottom triangles), although A is four times longer than B, it is ten times less noisy. The link B is particularly noisy between 10 and 1000 s integration time. Except for link B, the short term noise is limited by the finite propagation time of the light in the fiber [27].

The 705 km link (link C, blue circles) is affected by a pseudo-periodic perturbation of 10–100 s that degrades the MDEV. This perturbation may be due to the air conditioning and acoustic noise at the departing node in Paris, at mid-point and/or at the remote end of the cascaded link. For the three other links, we do not observe such perturbations.

At 40 000 s integration time the MDEV are 6×10^{-21}, 2×10^{-20}, 5×10^{-20}, 6×10^{-20} for the links A to D respectively. At one day, all four links show a bump, due to the diurnal variation of temperature affecting the Michelson interferometers of the RLSs and MLS2 or MLS3 [2, 35]. The excess of long-term noise on

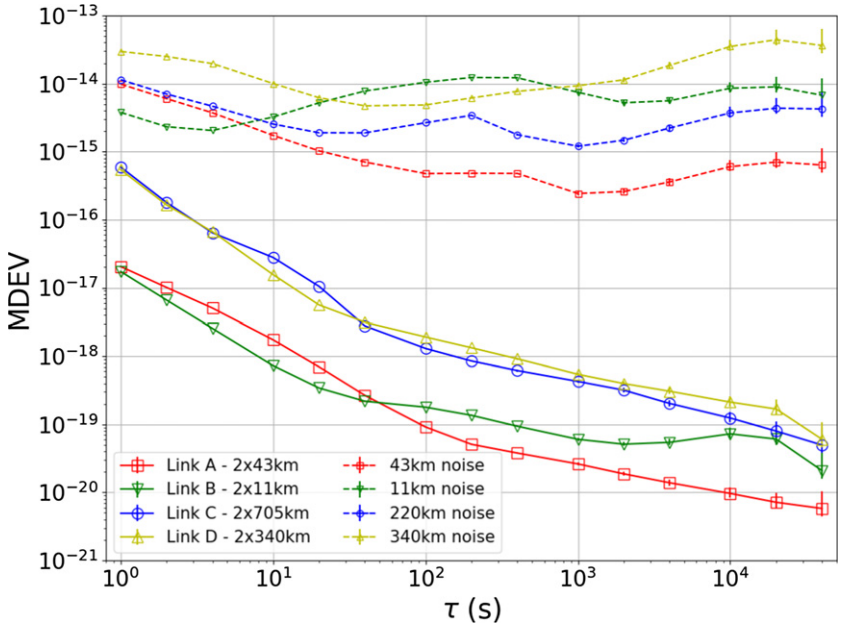

Figure 6. Stability (MDEV) of the four links using MLSs, for the data displayed on figure 5, together with the free-running stability of the first span of each links.

Table 2. Uptime (see section 4.3) and uncertainty of the four links using MLSs for the data displayed on figures 5 and 6. OADEV and MDEV are given at 40 000 s integration time.

	Uptime (%)	Mean ($\times 10^{-20}$)	OADEV ($\times 10^{-20}$)	MDEV ($\times 10^{-20}$)
A: SYRTE–LPL–SYRTE	97.3	0.4	0.9	0.6
B: SYRTE–Paris–SYRTE	97.9	−1.1	5.0	2.1
C: Paris–Strasbourg–Paris	98.1	−2.3	10.2	5.0
D: Paris–Lille–Paris	93.0	1.1	10.9	6.0

link B is due to the imperfect balance of the non-common paths and to the thermal sensitivity of the acousto-optic modulator set inside the TH2 interferometric ensemble. It copies the noise floor shown in figure 4 with a factor 2 amplification due to the double sensitivity to interferometric noise of a cascaded link, compared to a two-way measurement.

We can note a significant variation of the short-term phase noise of the 340 km link (link D, yellow) which reduces generally during the night (here observed between 1:30 and 6:00 UTC). As the data were acquired simultaneously with those of the three other links we can exclude instrumental effects related to the lasers or the electronics used in the MLS. It possibly comes from a diminution of the traffic along the highway near the path of the fibers or from any interruption of a noise source along the fiber. If the origin of the noise cannot yet be elucidated in our fiber network, this is a striking example of the non-stationarity of the short-term noise that affects ultra-stable fiber links.

4.2. Accuracy

In order to evaluate the fractional frequency offset of the frequency transfer, we calculate the mean relative frequency for these data sets, no corrections being applied to the data. By varying the frequency of the local oscillator of MLS2, we first verified that the transferred frequency is not affected by this local RF oscillator, which is thus not a limit for the uncertainty of the frequency transfer.

The uncertainty budget is therefore given by the statistical uncertainty, estimated by using the overlapping Allan deviation (OADEV) at 40 000 s. The values are reported in table 2. We evaluate the residual offset of the frequency transfer of the above data set as $(0.4 \pm 0.9) \times 10^{-20}$, $(-1.1 \pm 5) \times 10^{-20}$, $(-2.3 \pm 10.2) \times 10^{-20}$, $(1.1 \pm 10.9) \times 10^{-20}$, for links A to D respectively. No significant deviation of the mean is observed. Lower residual offsets can be obtained after extensive data analysis and dedicated link optimization.

This accuracy fully satisfies the requirements of the REFIMEVE project, and complies with the roadmap defined by the CCTF of BIPM for the future redefinition of the SI second at the level of 10^{-18}.

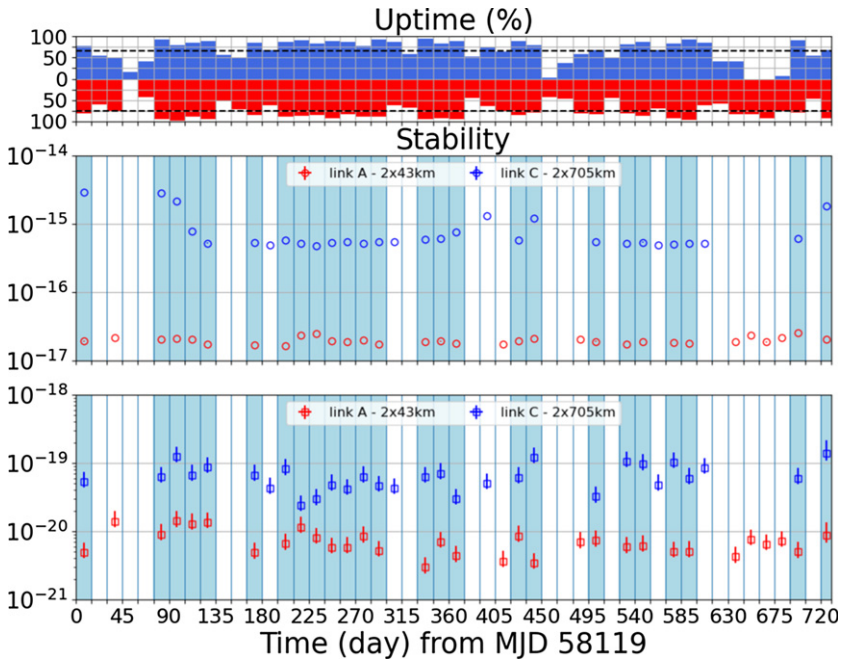

Figure 7. Uptime and stabilities over 2 years of two links departing from an MLS. The period is divided into bins of 15 days. Data concerning the Paris–Strasbourg–Paris link (link C) are in blue, and the ones concerning the SYRTE–LPL–SYRTE link (link A) in red. The circles correspond to stabilities at 1 s averaging time and the squares at 100 000 s. These stabilities are calculated for bins with uptime greater than the mean uptime, 75% and 66% for links A and C respectively (black dotted lines on upper graph). Data meeting these criteria are highlighted in sky blue in the lower graphs.

4.3. Network operation at a yearly scale

We now show the results of the operation of the links A (2 × 43 km) and C (2 × 705 km) during two years after the in-field set-up, from 2018-01-01 to 2019-12-31 using the three MLSs introduced above Over such a long period, there is missing data that are due to technical failure and to interruption of the service for maintenance, fiber operation or upgrade.

We first define the uptime of a link as the ratio between validated data points, estimated as a successful optical frequency transfer, and the total number of data points. This observable is therefore dependent on the criteria chosen to validate data. The uptime shown here is for the entire system composed of the ultra-stable cavity, the comb and the fiber link. The uptimes for the data shown in figure 5 are displayed in table 2. They are significantly above 90% since we chose a good functioning period of the four links.

For the two-year period, we process the end-to-end data with the three steps procedure described in [37]. First, we reject outliers, for which the norm of the relative frequency is 20 to 100 times larger than the short-term stability of the link. Then we process the data by calculating the rolling mean and rolling standard deviation over a time window of 10 s and 2800 s respectively. The parameters of the filters are tuned for each of the two links. We check that short-term stability and coherence of the links are kept, so that the frequency delivered to the remote end of the network can be used effectively by the users. For the two-year period, the uptime of the 86 km link (A, red) and 1410 km link (C, blue) are presented in figure 7. One bar of the histogram is the uptime calculated over 15 days, in red for link A and in blue for link C.

For the link A (SYRTE–LPL–SYRTE), the total uptime over the two years reaches 75%. It is more than 47 million seconds of frequency comparison. It is mainly limited by two regions of non-operation, from modified Julian day (MJD) 58161 to 58185, where the power supply of the MLS1 at LNE-SYRTE broke down and from MJD 58569 to 58599, where some upgrades of the optical reference were performed. The 6 months from MJD 58314 to 58494 presents an impressive uptime of 85%.

For the link C (Paris–Strasbourg–Paris), the total uptime over the two years is 66%. It is more than 41 million seconds of frequency comparison. The downtime periods of this link often coincide with that of the link A, except for the region between MJD 58764 and MJD 58809 where an upgrade of the link C' amplifiers has been realized. The uptime of the 6 months between MJD 58314 to 58494 is 85%. This last value is similar to that of the other link, emphasizing the fact the links are mostly limited by common sources of interruption.

The contributions of the downtime were investigated in details for the period between MJD 58119 and 58468, thanks to the remote control and logs of all the equipment in the network. The replacement of the electrical supply of the electronic boards of MLS1 in LNE-SYRTE is the main contributions of the

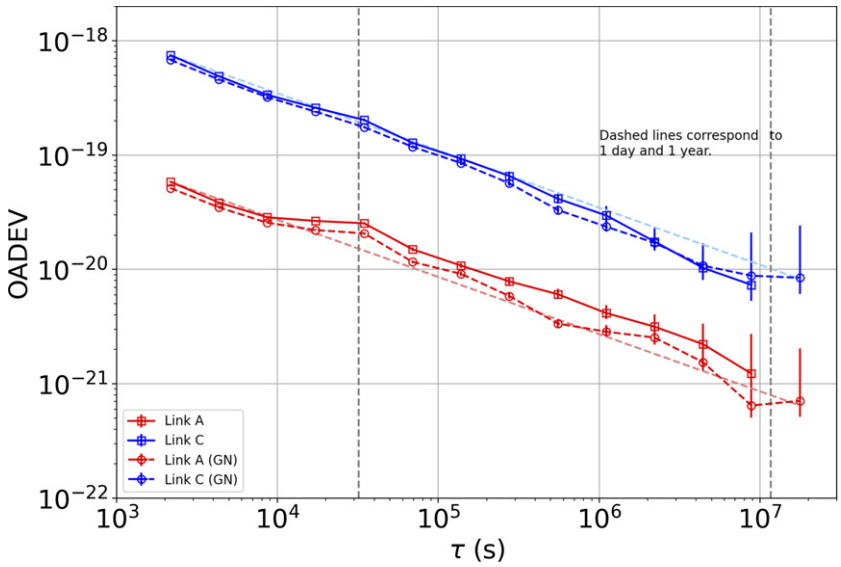

Figure 8. Long-term stability (OADEV) of the SYRTE–Strasbourg–SYRTE link (C, solid line and blue squares) and the SYRTE–LPL–SYRTE link (A, solid line and red squares) calculated from the averaged frequencies on periods spanning 2160 s. 31% and 47% of the data have been removed for links A and C respectively. Dotted lines follow a slope of $\tau^{-1/2}$ (represented by the dashed lines in light blue and red). Dotted lines and circles show the long-term stability when removed data were replaced by Gaussian noise. Dashed vertical lines correspond to the position of the bump expected for sinusoidal frequency fluctuations with periods 1 day and 1 year respectively.

downtime for both links. It represents 47% and 35% of the downtime of this period for the links A and C respectively. The second contribution comes from the interruptions of the phase/frequency counters that give the end-to-end measurement. This contributes to 30% and 25% of the downtime of this period for the links A and C respectively. The remainder of 23% and 40% for the links A and C respectively comes from several different contributions: the availability of the ultra-stable cavity, the network installation and maintenance, the adjustment of the polarization and interruptions of the 10 MHz reference. We are confident that the uptime can reach up to 90% and even close to 99% for the upcoming years.

Figure 7 shows the corresponding stabilities at 1 s and at 100 000 s integration time. We observe that the short-term stability of the 1410 km link (C) varies over months and is higher during winter, whereas it is approximately stationary for the 86 km link (A). At long term we observe repeatable results for both links, from 2×10^{-20} to 14×10^{-20} for the longest link and 3×10^{-21} to 14×10^{-21} for the shortest link.

4.4. Long term stability at a yearly scale

Finally, we use the 63 million points to calculate the long-term stabilities of the links A and C. After filtering the data with the procedure described above [37], we add a test condition on the mean value at 1000 s integration time to be below 10^{-18}. Then, we subdivide the data set in subsets of 2160 s, leading to 40 subsets per day. At 2160 s measurement time, the links are no longer in the coherent regime. The dominant noise is white frequency noise.

For each subset, we then calculate the mean frequency and the associated uptime. We consider any subset with an uptime higher than 90% as validated data. With this criterion, we keep 69% and 53% of the data for links A and C respectively. We then associate the resulting mean to a 2160 s measurement time. With this procedure, the missing data with small durations compared to 2160 s are handled with equivalent noise present in the given subset. For larger gaps, the subsets are simply handled as missing data or filled with a Gaussian noise model, not to perturb the stability at short integration time.

We check that the optical phase behaves steadily over the 2 years integration period and that the behavior does not depend critically on the uptime criteria of 90%. When processing the data with an uptime criterion of 99%, we remove only 34% and 53% of the data for links A and C respectively and obtain similar stabilities as shown in the supplementary material.

We then calculate the OADEV of the resulting collection of mean frequencies. It is displayed in figure 8, with red and blue squares for the A and C links respectively, together with the stabilities obtained when replacing the removed data with Gaussian noise (red and blue circles respectively).

As expected, we observed that the latter stability follows a slope of $\tau^{-1/2}$ as underlined by the light dashed lines. It is also approximately the case for the stability of the filtered collection of mean frequencies. We obtain long-term stabilities of 1.2×10^{-21} and 7×10^{-21} for the links A and C respectively. We also

calculate the mean of the mean frequencies. Despite the amplitudes of those means and stabilities should be taken carefully with such methodology, we thus estimate the fractional offset of the frequency transfer to $(-3 \pm 2) \times 10^{-21}$ $(-0.5 \pm 1) \times 10^{-20}$ for the links A and C respectively. This accuracy shows the robustness of the two links operated simultaneously with our MLS. Note that residual offset of link A is not significant because it is only 1.5 times the $1 - \sigma$ uncertainty, and could be due to non reciprocal effects or to residual effects of the data processing.

We observe one small bump, at integration time around 30 000 s in the OADEV of the shorter link A. On the longer link C, no clear bump is observed.

By comparing with a simulation, we found that the bump corresponds to a periodic noise of period approximately 1 day. In order to confirm this time period, we calculated the autocorrelation of the mean frequency. In that stage, there is no filtering on the uptime to preserve the time coherence of the data, giving more reliability to this method. We obtained a similar result of a periodic perturbation at 1 day. The detailed study of the long-term behavior and corresponding methods is beyond the scope of the paper.

5. Conclusion and perspectives

We present in this article MLSs that enable the building of fiber networks with excellent phase stability between the branches.

Three models were built. We presented the performances of the inner branches and branches-to-branches optical phase stability. We show that a simple temperature correction can improve the results by a factor of 30 and finally reach the 2.5×10^{-23} relative frequency stability. These results are state of the art.

The three MLSs were set up in the network. We present the simultaneous operation of the core of the REFIMEVE+ network with four branches. It demonstrates the viability of our approach for building coherent fiber networks.

The reliability of the network is studied in details, and thanks to the supervision of our network, causes for dysfunction are analyzed. We show an uptime of 85% over 6 months for a cascaded link of 1410 km. We conclude that 90% uptime over 1 year can be reached in the near future.

We report for the first time the operation of a metrological network, with four branches and a record range of 2198 km in total. We report frequency dissemination capabilities that matches the accuracy and stability specification of REFIMEVE+ and of the comparisons of any clock built to date. For the first time, to the best of our knowledge, relative frequency stability of a frequency network at long term is presented, until an integration time of 10^7 s. This integration time is two orders of magnitude larger than any other experimental results reported so far, and comparable to studies reported with satellite means. This work is a major step towards reliable optical frequency dissemination over fiber networks, and gives important credit for such new research infrastructures, enabling new scientific opportunities for precise spectroscopy and for a wide scope of research laboratories and research communities, concerned by chronometric geodesy, dark matter hunt, gravitational wave detection and very long baseline interferometry.

Funding

Program 'Investissements d'Avenir' launched by the French Government and implemented by Agence Nationale de la Recherche with references Labex First-TF ANR-10-LABX-48-01, Equipex REFIMEVE+ ANR-11-EQPX-0039, ANR-10-IDEX-0001-002 PSL, Conseil Régional Bourgogne-Franche-Comté, Conseil Régional Ile de-France (DIM IFRAF), the European Metrology Program for Innovation and Research (EMPIR) in Project 15SIB05 (OFTEN). The EMPIR is jointly funded by the EMPIR participating countries within EURAMET and the European Union.

Data availability statement

The data that support the findings of this study are available upon reasonable request from the authors.

Acknowledgments

We acknowledge unfailing and continuing support of the network and engineering team of RENATER, and especially Nicolas Quintin, Xavier Misseri, Laurent Gydé and Emilie Camisard. We also acknowledge Michel Abgrall and Hector Alvarez for providing us with the ultra-stable and accurate optical signal generated at

LNE-SYRTE. We also acknowledge support of Fabrice Wiotte and Albert Kaladjian for the building of the MLS. We acknowledge Yann Kersalé for providing us with RIO diode lasers. Finally, we acknowledge Giorgio Santarelli for fruitful discussions and Christian Chardonnet for continuing support.

ORCID iDs

Etienne Cantin https://orcid.org/0000-0001-9362-0628
Mads Tønnes https://orcid.org/0000-0002-3630-3121
Rodolphe Le Targat https://orcid.org/0000-0002-8740-1709
Anne Amy-Klein https://orcid.org/0000-0002-5122-7868
Olivier Lopez https://orcid.org/0000-0003-3171-2863
Paul-Eric Pottie https://orcid.org/0000-0003-3677-2208

References

[1] Calonico D *et al* 2014 High-accuracy coherent optical frequency transfer over a doubled 642 km fiber link *Appl. Phys.* B **117** 979–86
[2] Chiodo N *et al* 2015 Cascaded optical fiber link using the internet network for remote clocks comparison *Opt. Express* **23** 33927–37
[3] Raupach S M F, Koczwara A and Grosche G 2015 Brillouin amplification supports 1×10^{-20} uncertainty in optical frequency transfer over 1400 km of underground fiber *Phys. Rev.* A **92** 021801
[4] Koke S *et al* 2019 Combining fiber Brillouin amplification with a repeater laser station for fiber-based optical frequency dissemination over 1400 km *New J. Phys.* **21** 123017
[5] Clivati C *et al* 2020 Common-clock very long baseline interferometry using a coherent optical fiber link *Optica* **7** 1031–7
[6] Xu D, Delva P, Lopez O, Amy-Klein A and Pottie P-E 2019 Reciprocity of propagation in optical fiber links demonstrated to 10^{-21} *Opt. Express* **27** 36965–75
[7] Lisdat C *et al* 2016 A clock network for geodesy and fundamental science *Nat. Commun.* **7** 12443
[8] Takano T *et al* 2016 Geopotential measurements with synchronously linked optical lattice clocks *Nat. Photon.* **10** 662–6
[9] McGrew W F *et al* 2018 Atomic clock performance enabling geodesy below the centimetre level *Nature* **564** 87
[10] Delva P *et al* 2017 Test of special relativity using a fiber network of optical clocks *Phys. Rev. Lett.* **118** 221102
[11] Friebe J *et al* 2011 Remote frequency measurement of the $^1S_0 \rightarrow {}^3P_1$ transition in laser-cooled ^{24}Mg *New J. Phys.* **13** 125010
[12] Matveev A *et al* 2013 Precision measurement of the hydrogen 1S − 2S frequency via a 920 km fiber link *Phys. Rev. Lett.* **110** 230801
[13] Argence B *et al* 2015 Quantum cascade laser frequency stabilization at the sub-Hz level *Nat. Photon.* **9** 456–60
[14] Insero G *et al* 2017 Measuring molecular frequencies in the 1–10 μm range at 11-digits accuracy *Sci. Rep.* **7** 12780
[15] Santagata R *et al* 2019 High-precision methanol spectroscopy with a widely tunable SI-traceable frequency-comb-based mid-infrared QCL *Optica* **6** 411–23
[16] Clivati C, Calonico D, Costanzo G A, Mura A, Pizzocaro M and Levi F 2013 Large-area fiber-optic gyroscope on a multiplexed fiber network *Opt. Lett.* **38** 1092–4
[17] Clivati C, Tampellini A, Mura A, Levi F, Marra G, Galea P, Xuereb A and Calonico D 2018 Optical frequency transfer over submarine fiber links *Optica* **5** 893–901
[18] Marra G *et al* 2018 Ultrastable laser interferometry for earthquake detection with terrestrial and submarine cables *Science* **361** 4458
[19] Clivati C *et al* 2017 A VLBI experiment using a remote atomic clock via a coherent fibre link *Sci. Rep.* **7** 40992
[20] Roberts B M *et al* 2020 Search for transient variations of the fine structure constant and dark matter using fiber-linked optical atomic clocks *New J. Phys.* **22** 093010
[21] Grosche G 2014 Eavesdropping time and frequency: phase noise cancellation along a time-varying path, such as an optical fiber *Opt. Lett.* **39** 2545
[22] Bercy A, Guellati-Khelifa S, Stefani F, Santarelli G, Chardonnet C, Pottie P-E, Lopez O and Amy-Klein A 2014 In-line extraction of an ultrastable frequency signal over an optical fiber link *J. Opt. Soc. Am.* B **31** 678–85
[23] Bercy A, Lopez O, Pottie P-E and Amy-Klein A 2016 Ultrastable optical frequency dissemination on a multi-access fibre network *Appl. Phys.* B **122** 189
[24] REFIMEVE+ project, http://refimeve.fr/index.php/en/
[25] Guillou-Camargo F *et al* 2018 First industrial-grade coherent fiber link for optical frequency standard dissemination *Appl. Opt.* **57** 7203–10
[26] Lodewyck J *et al* 2016 Optical to microwave clock frequency ratios with a nearly continuous strontium optical lattice clock *Metrologia* **53** 1123–30
[27] Newbury N R, Williams P A and Swann W C 2007 Coherent transfer of an optical carrier over 251 km *Opt. Lett.* **32** 3056
[28] Lopez O, Haboucha A, Kéfélian F, Jiang H, Chanteau B, Roncin V, Chardonnet C, Amy-Klein A and Santarelli G 2010 Cascaded multiplexed optical link on a telecommunication network for frequency dissemination *Opt. Express* **18** 16849–57
[29] Delva P *et al* 2017 Test of special relativity using a fiber network of optical clocks *Phys. Rev. Lett.* **118** 221102
[30] Hanson D W 1989 Fundamentals of two-way time transfers by satellite *Proc. of the 43rd Annual Symp. on Frequency Control* pp 174–8
[31] Calosso C E, Bertacco E, Calonico D, Clivati C, Costanzo G A, Frittelli M, Levi F, Mura A and Godone A 2014 Frequency transfer via a two-way optical phase comparison on a multiplexed fiber network *Opt. Lett.* **39** 1177–80
[32] Rubiola E 2005 On the measurement of frequency and of its sample variance with high-resolution counters *Rev. Sci. Instrum.* **76** 054703
[33] Dawkins S T, McFerran J J and Luiten A N 2007 Considerations on the measurement of the stability of oscillators with frequency counters *IEEE Trans. Ultrason. Ferroelectr. Freq. Control* **54** 918–25

[34] Williams P A, Swann W C and Newbury N R 2008 High-stability transfer of an optical frequency over long fiber-optic links *J. Opt. Soc. Am.* B **25** 1284–93
[35] Stefani F, Lopez O, Bercy A, Lee W-K, Chardonnet C, Santarelli G, Pottie P-E and Amy-Klein A 2015 Tackling the limits of optical fiber links *J. Opt. Soc. Am.* B **32** 787–97
[36] Wada M, Okubo S, Kashiwagi K, Hong F, Hosaka K and Inaba H 2018 Evaluation of fiber noise induced in ultrastable environments *IEEE Trans. Instrum. Meas.* **68** 2246–52
[37] Xu D, Cantin E, Frank F, Quintin N, Meynadier F, Tuckey P, Amy-Klein A, Lopez O and Pottie P-E 2019 Two-branch fiber link for international clock networks *IEEE Trans. Instrum. Meas.* **68** 2195–200